

Review

Aqueous Organic Redox-Targeting Flow Batteries with Advanced Solid Materials: Current Status and Future Perspective

Jin Ma, Sida Rong, Yichong Cai, Tidong Wang, Zheng Han and Ya Ji *

China-UK Low Carbon College, Shanghai Jiao Tong University, Shanghai 201306, China

* Correspondence: jiya@sjtu.edu.cn

Abstract: Aqueous organic redox flow batteries (AORFBs) represent innovative and sustainable systems featuring decoupled energy capacity and power density; storing energy within organic redox-active materials. This design facilitates straightforward scalability, holding the potential for an affordable energy storage solution. However, AORFBs face challenges of unsatisfied energy density and stability. Redox-targeting (RT) reaction is a promising way to resolve these problems, which involves a closed-loop electrochemical–chemical cycle between soluble redox mediators and solid materials. Among all these systems, the aqueous organic redox-targeting system is the most promising due to its greater sustainability, safety, low cost, and excellent tunability when compared to non-aqueous or all-vanadium systems, especially when it comes to energy storage on a large scale. Firstly, various types of AORFBs and their characteristics are discussed and analyzed, followed by introducing the concept and the evolution of RT. In addition, advanced characterization techniques to analyze RT-based AORFBs are summarized. Finally, the challenges lying in aqueous organic redox-targeting flow batteries are stated and corresponding recommendations are provided. It is anticipated that AORFBs with advanced solid materials will provide a promising solution for large-scale energy storage.

Keywords: aqueous organic redox flow batteries; redox-targeting reaction; advanced energy materials; potential matching; large-scale energy storage



Citation: Ma, J.; Rong, S.; Cai, Y.; Wang, T.; Han, Z.; Ji, Y. Aqueous Organic Redox-Targeting Flow Batteries with Advanced Solid Materials: Current Status and Future Perspective. *Sustainability* **2023**, *15*, 15635. <https://doi.org/10.3390/su152115635>

Academic Editor: Jiageng Ruan

Received: 28 September 2023

Revised: 2 November 2023

Accepted: 2 November 2023

Published: 5 November 2023



Copyright: © 2023 by the authors. Licensee MDPI, Basel, Switzerland. This article is an open access article distributed under the terms and conditions of the Creative Commons Attribution (CC BY) license (<https://creativecommons.org/licenses/by/4.0/>).

1. Introduction

The increasing energy demand, intensifying environmental issues, and the imperative for sustainability prompt the development of renewable energy, and will become the cornerstone of a modern energy system [1]. However, the intermittent nature of renewables such as solar energy and wind makes their deep penetration into the energy system difficult. This challenge has provoked a pressing necessity for developing safe, efficient and inexpensive grid-scale energy storage systems [2,3]. The most widely deployed grid-scale storage technology is pumped-storage hydropower (PSH), where the storage capacity accounts for over 90% of total global market [4,5]. However, the PSH technology is limited by specific geographical conditions, low power density and elevated costs of installation [6]. Thus, greater emphasis has been devoted to electrochemical energy storage systems with merits of geographical independence [7], high energy density, low cost and high efficiency [8,9]. Among various electrochemical energy storage systems, the redox flow battery (RFB) is a promising technology for a flexible, long life, and sustainable energy storage system [10]. Compared to conventional solid-state or static batteries, the RFB cell stack is detached from the electrolyte reservoirs, thereby achieving the power-capacity decoupling [11]. The power output is contingent upon the electrode area, whereas the capacity is governed through the concentration and magnitude of the electrolyte tanks [12,13]. This merit offers the RFB not only scaling flexibility, but also great safety without thermal runaway. There are two types of RFBs based on solvent used, non-aqueous and aqueous. Even though non-aqueous RFBs have a high voltage range, they are facing unavoidable challenges, such as poor ion

conductivity, flammability and toxicity relevant to organic solvents [9,12]. Thus, aqueous RFBs with advantages of safety, cost-effectiveness and environmental friendliness are more attractive for applications involving extensive energy storage.

At this early stage, most RFBs employ metal-based redox couples as electrochemically active materials like iron, chromium, and vanadium ions. Vanadium redox flow batteries (VRFBs) are the most widespread technologies, and employ vanadium ions with different valence states as posolyte ($\text{VO}^{2+}/\text{VO}_2^+$) and negolyte ($\text{V}^{2+}/\text{V}^{3+}$) without cross-contamination issues [14,15]. Although VRFBs demonstrate exceptional long-term cycling stability and high energy efficiency [16], metal-based RFBs have several disadvantages, including limited metal reserves, high cost, strong corrosiveness of electrolytes, limited membrane selection, and slow kinetics [17,18]. These drawbacks hinder their large-scale commercialization applications. Therefore, researchers are increasingly focusing on inexpensive, widely available, and structurally controllable organic molecules as the redox-active electrolyte species for AORFBs which operate on similar principles to VRFBs, but utilize water-soluble organic compounds that consist of elements abundant in the Earth [19,20]. The advent of AORFBs paves the way for pioneering advancements in the realm of next-generation RFBs, characterized by heightened safety, cost-effectiveness, and superior energy storage capabilities. The remarkable assortment and effortless structural modifications of these organic compounds bear significance in tunable properties such as solubility in water [21], kinetics of redox reactions, redox potential, and overall stability [22,23].

However, similar to other RFB systems, AORFBs have limited energy density owing to the low solubility of organic mediators [24]. To solve this problem, researchers explore many strategies to enhance the energy density of RFBs. Such strategies include extending the voltage [25], maximizing the solubility of active materials [26], utilizing multi-electron transfer processes [27], developing semisolid flow batteries and designing redox-targeting (RT) based system [28,29]. Among these different strategies, redox-targeting based RFBs stand out by using redox mediators (RMs) as electron shuttles between electrode and energy storage solid materials (solid materials) in electrolyte tanks, storing energy in solid materials instead of soluble molecules in conventional RFBs. Redox-targeting based RFBs breaks the boundary of solid phase and liquid phase energy storage, providing a captivating methodology for bulk energy storage.

In this review, we focus our attention on the redox-targeting aqueous organic redox flow batteries (RT-AORFBs). Currently, there are several articles based on redox-targeting systems, which mainly discussed inorganic RT systems composed of inorganic RMs or solid materials. All-organic RT redox flow batteries are not comprehensively reviewed yet. This review will discuss in detail the most up-to-date articles based on redox-targeting based aqueous organic RFBs. The first part of this review will address advances and challenges in AORFBs. Then, the evolution of redox-targeting systems will be introduced followed by current research progress in redox-targeting based AORFBs. Lastly, we will wind up with a summary of current sustainability challenges and prospects in RT-based redox flow batteries.

2. Aqueous Organic Redox Flow Batteries

During the past decade, there has been a substantial amount of attention and notable advancements in the field of AORFBs that utilize water-soluble organic compounds [30]. Organic RMs offer several advantages, including abundant elements, reduced environmental footprint, and the potential for cost-effectiveness. The designability of these materials allow for precise tuning of their structures and chemical properties. For instance, the introduction of electron-donating (OH^-) can respectively shift the redox potential in the negative directions [31]. Additionally, the incorporation of ammonium groups has been shown to enhance both solubility and electrochemical reaction rates. Furthermore, aqueous electrolytes, consisting of water, when used in conjunction with selective ion-conductive membranes offer numerous benefits, such as enhanced safety, cost-effectiveness, greater

alignment with sustainability goals, and enhanced ionic conductivity, resulting in higher energy conversion efficiency. A key advantage, when compared to VRFBs, is that it exhibits superior reversibility in the redox processes and electron transfer rate.

In 2014, Aziz et al. proposed an anthraquinone-based AORFB, and it sparked research areas of keen interest in the field of RFBs [32]. After that, numerous studies have focused on the advancement of innovative RMs within alkaline, acidic, or neutral pH solutions. Figure 1 summarizes typical posolytes and negolytes under different pH conditions. In acidic conditions, anthraquinones (AQ) with potentials (0.1 V~0.3 V vs. SHE) are commonly used as negolytes while benzoquinones and phenothiazines (0.5 V~0.9 V vs. SHE) work as posolytes. In neutral or near neutral conditions, anthraquinones, phenazines, and viologens (−0.2 V~−0.6 V vs. SHE) are used as negolytes when ferrocenes and tetramethyl-1-piperidinyloxys (TEMPOs) (0.3 V~1.1 V vs. SHE) work as posolytes under mild pH conditions. In alkaline conditions, anthraquinones, benzoquinones and phenazines (−0.5 V~−0.8 V vs. SHE) are frequently selected as negolytes while few molecules are reported as posolytes.

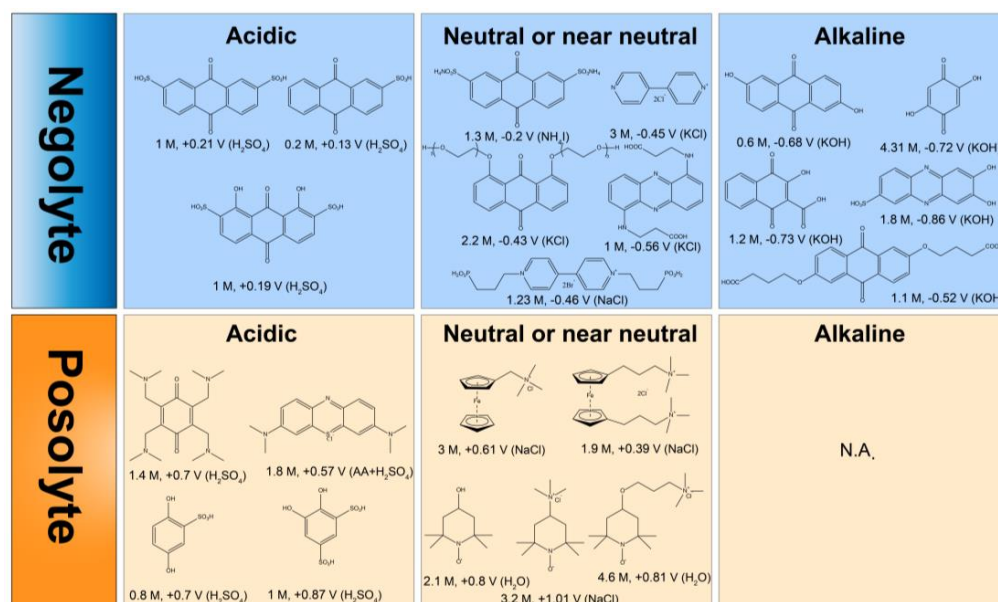


Figure 1. Typical organic posolytes and negolytes under different pH conditions.

2.1. Quinone Derivatives

Aziz et al. reported the unprecedented AQ-based AORFB system in acid conditions [32]. AQDS and Br₂ are employed as anolyte and catholyte in sulfuric acid solution. During charging and discharging, AQDS undergoes expeditious redox reaction (two-electron transfer) with a kinetic constant of 7.2×10^{-3} cm/s, which demonstrates a notably faster rate than vanadium ions. The cell exhibits an open-circuit voltage (OCV) and achieves a peak power density of 0.92 V and approximately 1.4 W/cm² when it is at a 90% state of charge (SOC). At 10% SOC, the OCV decreases to 0.69 V, but the peak power density increases to around 3.3 W/cm² (Figure 2a). Figure 2b shows that the capacity retention exceeds 99%, implying the battery exhibits minimal capacity degradation and high current efficiencies. Considering the high toxicity from bromine and the high corrosion from H₂SO₄, Marshak et al. put forth an alkaline AORFB with 2,6-dihydroxyanthraquinone (2,6-DHAQ) as the anolyte and ferro/ferricyanide as the catholyte in KOH (Figure 2c) [22]. As shown in Figure 2d, the cyclic voltammogram of the two redox-active molecules indicates a cell voltage of 1.2 V, along with OCV 1.34 V at 100% SOC. The high OCV compared with AQDS/Br₂ system is due to the deprotonated hydroxyl groups in alkaline conditions offering improved electron donation ability of AQ. Later, researchers modified the structure of AQs improving their stability and solubility. To mitigate the side reactions of AQ in

acidic and alkaline conditions, AQs in pH-neutral conditions were developed and applied in AORFBs. One example is the polyethylene glycol (PEG)-modified AQ, which is 1,8-bis(2-(2-(2-hydroxyethoxy)-ethoxy) ethoxy) anthracene-9,10-dione (AQ-1,8-3E-OH) [33]. This molecule showcases a remarkable solubility of 1.5 M in 1 M KCl. Which contributes to an impressive capacity of 80.4 Ah per liter and an exceptional energy density of 25.2 Wh per liter. As illustrated in Figure 2e, the battery delivers 1.21 V OCV and 140 mW/cm² peak power density when fully charged, with a negligible capacity loss of only 0.043% per cycle (Figure 2f). It is noted that the verified energy density of AQs is relatively lower in alkaline or acidic conditions than that in neutral solutions. Besides, AQs with diverse functional groups exhibit different chemical stability, causing good or bad capacity loss with battery cycling.

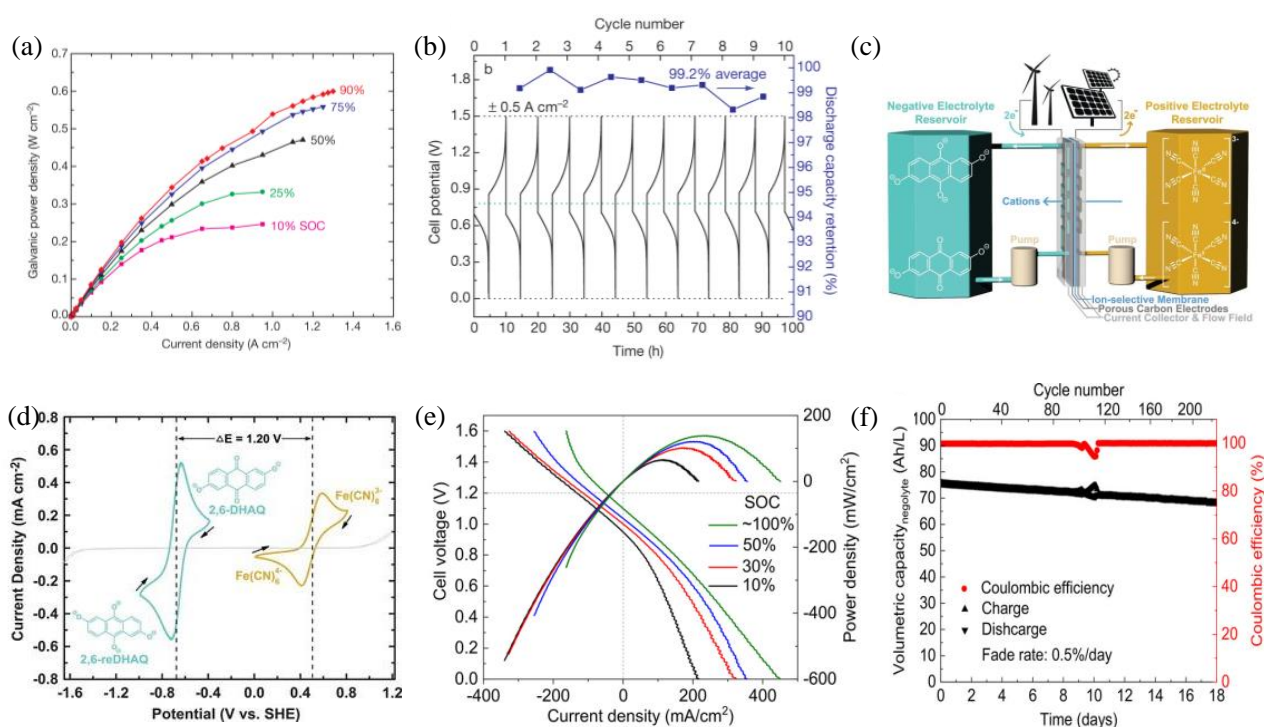


Figure 2. (a) The relationship between power density and current density at five distinct SOC levels with a solution containing 3 M HBr and 0.5 M Br₂ in the cathodic side, and a combination of 1 M AQDS and 1 M H₂SO₄ in the anodic side. (b) Discharge capacity retention and cell potential versus cycle number. (c) Illustration of the full battery during charging. (d) CV of 2 mM 2,6-DHAQ (the left one) and ferrocyanide (the right one). (e) Voltage profiles versus current density at ambient temperature at four distinct SOC levels. The electrolyte composition consists of 7 mL of 1.5 M PEGAQ. (f) The relationship between coulombic efficiency and time. (a,b), (c,d), (e,f) are reprinted with permissions from references [22,32,33].

2.2. TEMPO/Viologen Derivatives

Significant progress has been achieved concerning ORFBs operating in neutral aqueous media, utilizing (2,2,6,6-tetramethylpiperidin-1-yl) oxyl (TEMPO). TEMPO is widely used in organic polysolutes, and undergoes a rapid redox reaction (one-electron transfer) [34,35]. While being high, there is still room for substantial improvement to maximize the cell voltages in an aqueous RFB system well before reaching the point of oxygen evolution. However, TEMPO is insoluble in water. Liu et al. attached hydroxyl groups to the 4-positions yielding 4-OH-TEMPO, which exhibits a solubility of 2.1 M in water (Figure 3a) [36]. Through Equation (1) [37], it has been determined that the kinetic rate constant of 4-HO-TEMPO ($2.4 \times 10^{-3} \text{ cm s}^{-1}$) is comparable to that of vanadium ions ($5.3 \times 10^{-4} \text{ cm s}^{-1}$) [38,39], where i_0 represents the exchange current, F represents Fara-

day's constant, A represents the surface area of the working electrode, n represents the number of transferred electrons, and c represents the molar concentration. When employing methyl viologen (MV), the battery demonstrates an exceptionally elevated cell-voltage, measuring 1.25 V, and consistently maintains its capacity over 100 cycles with an almost perfect Coulombic efficiency, as illustrated in Figure 3b. However, the degradation of 4-OH-TEMPO does exist, particularly under acidic or alkaline conditions. This is attributed to the self-oxidation of the hydroxyl groups at the 4-position by the oxidized 4-OH-TEMPO. Therefore, changes in pH significantly affect TEMPO concentration, and these pH variations are induced through the consumption of OH ions in the TEMPOL⁺ (the oxidation form of TEMPO) reaction depicted in Figure 3c. Prior to electrochemical charging, TEMPOL⁺ may form under acidic conditions via a chemical reaction. At higher OH⁻ concentrations, it can chemically convert back to TEMPO, rendering TEMPO irreversible electrochemically in strongly alkaline electrolytes. This suggests that TEMPO should be employed in aqueous solutions close to neutral pH to avoid side reactions [37].

$$k_0 = i_0/nFA \quad (1)$$

To suppress such degradation of 4-OH-TEMPO, Janoschka et al. replaced OH with quaternary ammonium groups, and combined this with methyl viologen (MV), which demonstrated a remarkable capacity retention of almost 100% over 100 consecutive cycles, suggesting the robust electrochemical stability of N,N,N-2,2,6,6-heptamethyl piperidinyloxy-4-ammonium chloride (TEMPTMA) [40]. TEMPTMA exhibits an impressive solubility level, reaching 3.2 M in 0.3 M NaCl, which corresponds to a capacity of 85 Ah/L, respectively (Figure 3d). Recently, Seo et al. verified that the predominant cause of molecular decomposition is primarily attributed to the robust interaction between TEMPOL⁺ and OH ions. Then synthesized the MIMAcO-TEMPO (4-[2-(N-methyl imidazolium) acetoxy]-2,2,6,6-tetramethylpiperidine-1-oxyl chloride) with a hydroxide-philic functional group, which restricts the accessibility of OH⁻ ions to the oxoammonium sites [41]. As illustrated in Figure 3e, cell cycling results displayed a capacity fade rate of 0.012% per cycle and attained a discharge capacity of 57.1 Ah/L.

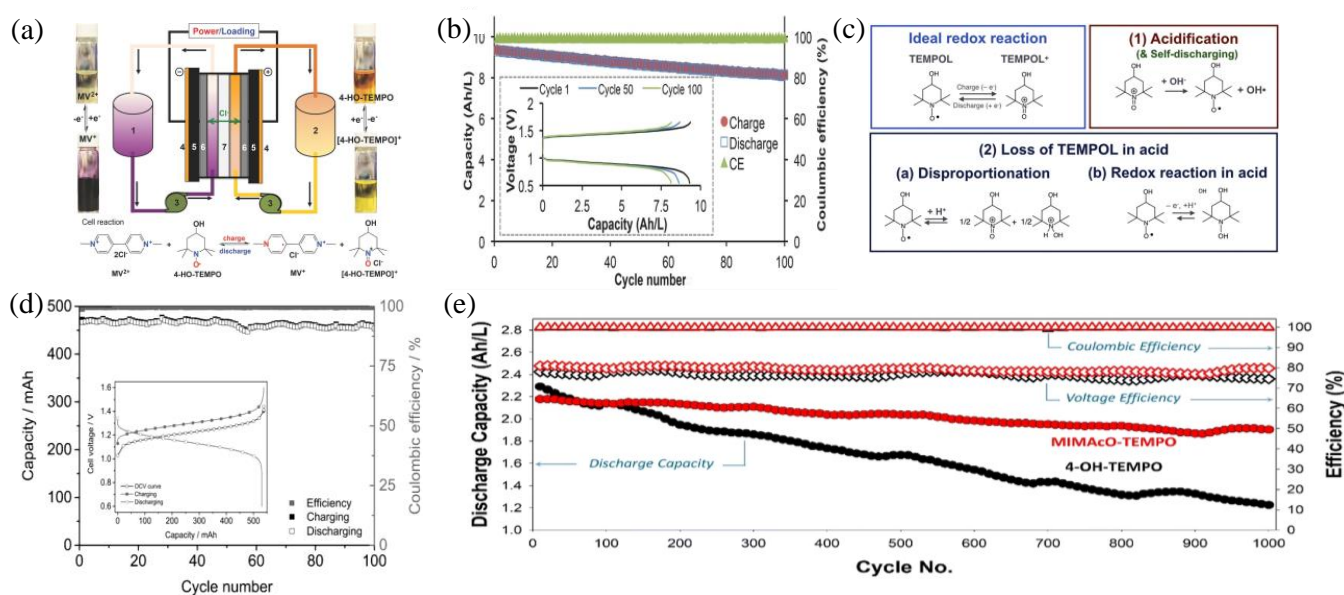


Figure 3. Cont.

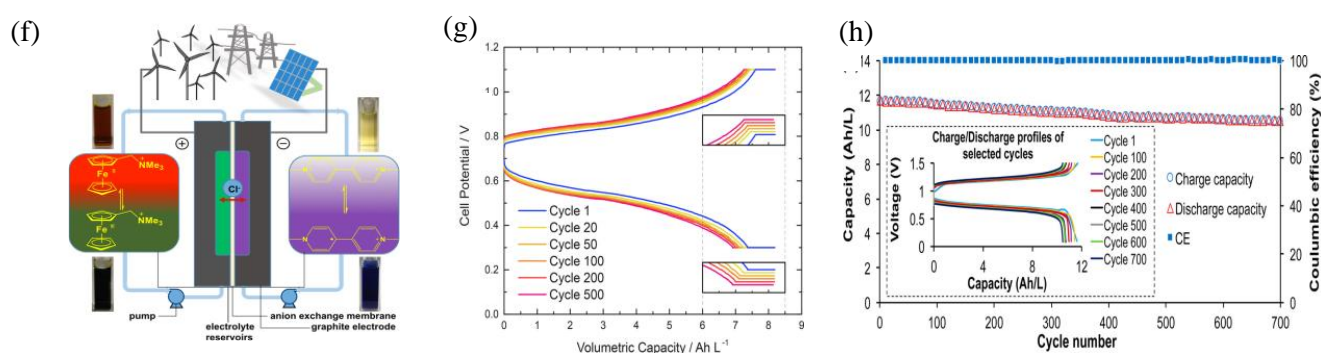


Figure 3. (a) An illustration of the MV/4-HO-TEMPO AORFB. (b) Capacity and voltage vs. cycle numbers. (c) The ideal reaction of TEMPOL, the loss of TEMPOL in acid with H^+ , and the acidification reaction of $TEMPOL^+$ with OH^- . (d) The durability assessment of the TEMPTMA/MV cell at room temperature. (e) Cycling of MIMAcO-TEMPO and 4-OH-TEMPO. (f) Schematic illustration of the FcNCl/MV cell and the discharged and charged states of them. (g) Cell potential versus cycle numbers of BTMAP-Vi/BTMAP-Fc AORFB. (h) The 700-cycle result of the 0.5 M FcNCl/MV AORFB: voltage and Coulombic efficiency versus time traces. (a,b), (c), (d), (e), (f,h) and (g) are reprinted with permissions from references [36,37,42–45].

2.3. Ferrocene Derivatives

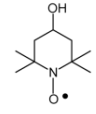
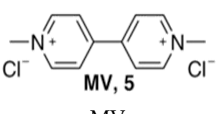
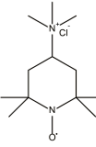
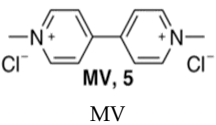
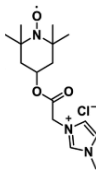
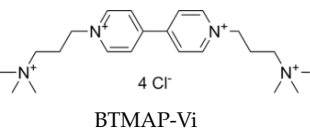
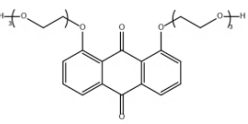
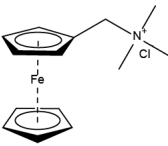
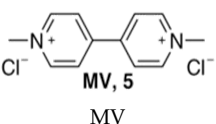
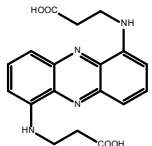
Ferrocene derivatives are highly redox-reversible molecules composed of two cyclopentadiene molecules with Fe-ion in the center [42,43]. The iron center undergoes a reversible one-electron transfer process, yielding a redox potential approximately 0.4 V. Thus, making ferrocene derivatives suitable as catholytes for AORFBs [46,47]. Nevertheless, ferrocene is hard to dissolve in water, hindering its direct application in AORFBs [48]. Thus, considerable dedication has been devoted to make water-soluble ferrocene derivatives. Liu et al. proposed water-soluble derivatives of ferrocene unprecedentedly by modifying ferrocene with quaternary ammonium groups, namely (ferrocenylmethyl) trimethylammonium chloride (FcNCl) and N^1 -ferrocenylmethyl- N^1,N^1,N^2,N^2,N^2 -pentamethylpropane-1,2-diaminium dibromide (FcN₂Br₂) [49]. By introducing the hydrophilic functional groups, solubility of FcNCl in water can reach 4.0 M, while that of FcN₂Br₂ is 3.1 M. Therefore, greatly enhancing the capacity of ferrocene derivatives. The battery consisting of FcNCl/methyl viologen delivers an OCV and power density of 1.06 V and approximately 125 mW/cm² (Figure 3f). Furthermore, the theoretical energy density of this particular battery is up to 45.5 Wh/L. At 0.5 M, the FcNCl/MV cell exhibited a daily capacity degradation rate of 0.58% (Figure 3g). However, the capacity decline was considerably faster at 0.7 M, with a daily decrease rate of 1.3%. To address the decomposition, Aziz et al. introduced a pair of quaternary ammonium groups, resulting in the synthesis of BTMAP-Fc, which displayed an impressive water solubility of 1.9 M and a decreased membrane permeation rate for its increased size [44]. This battery utilizes a novel organic molecule as an electrolyte, enabling efficient charge storage and discharge under neutral pH conditions. This innovative battery design holds the promise of addressing environmental and safety concerns associated with traditional flow batteries employing acidic or alkaline electrolytes while delivering higher energy density and cycle life. The daily capacity retention rate was upheld at an impressive 99.967% at 0.75 M (Figure 3h). This not only addresses decomposition but also allows the battery to operate under neutral conditions. It maintains electrical conductivity while being environmentally friendly and non-corrosive to the equipment.

2.4. Challenges of Conventional AORFBs

Despite a series of pioneering studies demonstrating favorable electrochemical performance, the advancement of AORFBs still presents numerous known and unknown challenges (Table 1). Firstly, the energy density of AORFBs has not yet exceeded that of their competing VRFBs. This discrepancy can be attributed to the comparatively lower

solubility and electrochemical potential of organic RMs in comparison to VRFBs. The limited solubility of organic RMs (such as quinone, TEMPO, fluorenone, viologen, phenazine, and alloxazine) poses a significant obstacle to enhancing energy density. While numerous promising organic RMs have been created for AORFBs, the majority have only been tested at restricted concentrations (below 0.5 M). Secondly, the potential for crossover of the electrolytes still exists, which can result in a decline in capacity and energy, thereby diminishing the lifetime of the AORFB system. Lastly, the observed capacity degradation-rate falls short of the stability criteria necessary for large-scale applications.

Table 1. Summary of AORFBs in terms of cell tests and current issues encountered.

Catholyte	Anolyte	Performance	Problem	Ref.
 4-HO-TEMPO	 MV, 5 MV	<ul style="list-style-type: none"> •1.25 V cell voltage •43.2 Ah/L capacity •89% capacity retention in 100 cycles 	<ul style="list-style-type: none"> •The degradation of 4-OH-TEMPO •Only for neutral conditions 	[35]
 TEMPTMA	 MV, 5 MV	<ul style="list-style-type: none"> •1.4 V cell voltage •54 Ah/L capacity •96.3% capacity retention in 100 cycles 	<ul style="list-style-type: none"> •Relatively complex synthesis steps of TEMPTMA •Low energy density 	[39]
 MIMAcO-TEMPO	 4 Cl ⁻ BTMAP-Vi	<ul style="list-style-type: none"> •1.18 V cell voltage •57.1 Ah/L capacity •88.3% capacity retention in 1000 cycles 	<ul style="list-style-type: none"> •Slow kinetics •High internal resistance of the membrane 	[40]
 PEGAQ	$K_4 [Fe(CN)_6]$	<ul style="list-style-type: none"> •1.0 V cell voltage •80.4 Ah/L capacity •95.8% capacity retention in 100 cycles 	<ul style="list-style-type: none"> •The decomposition of PEGAQ •Relatively complex synthesis steps of PEGAQ 	[32]
 FeNCl	 MV, 5 MV	<ul style="list-style-type: none"> •1.06 V cell voltage •107.2 Ah/L capacity •93.2% capacity retention in 100 cycles 	<ul style="list-style-type: none"> •Low energy density •Slow kinetics •High toxicity 	[48]
 2,6 DAEAQ	$K_4 [Fe(CN)_6]$	<ul style="list-style-type: none"> •1.12 V cell voltage •58.76 Ah/L capacity •91.3% capacity retention in 100 cycles 	<ul style="list-style-type: none"> •Stringent pH restrictions •Low volumetric capacity 	[31]

3. Evolution of Redox-Targeting Based System

3.1. Concept and Principles

The concept of redox-targeting (RT) was first introduced in 2006 to address the solubility issues encountered in the AORFB system. This concept originates from both molecular wiring and polymer wiring, such as in the case of $LiFePO_4$. $LiFePO_4$ itself exhibits poor electronic conductivity, necessitating the incorporation of a substantial amount of carbon black to form a continuous conductive network for electron penetration. However, the inclusion of a large quantity of non-active conductive agents significantly diminishes the power density of the system. Therefore, Wang et al. sought to introduce a chemisorbed

monolayer of redox-active molecules on its surface, attempting molecular wiring of the battery material (Figure 4a) [29]. Figure 4b shows that the electrode materials can be stored in individual tanks and electrochemically accessed through the surrounding redox relay. Notably, the omission of conducting additives is anticipated to significantly enhance the energy density.

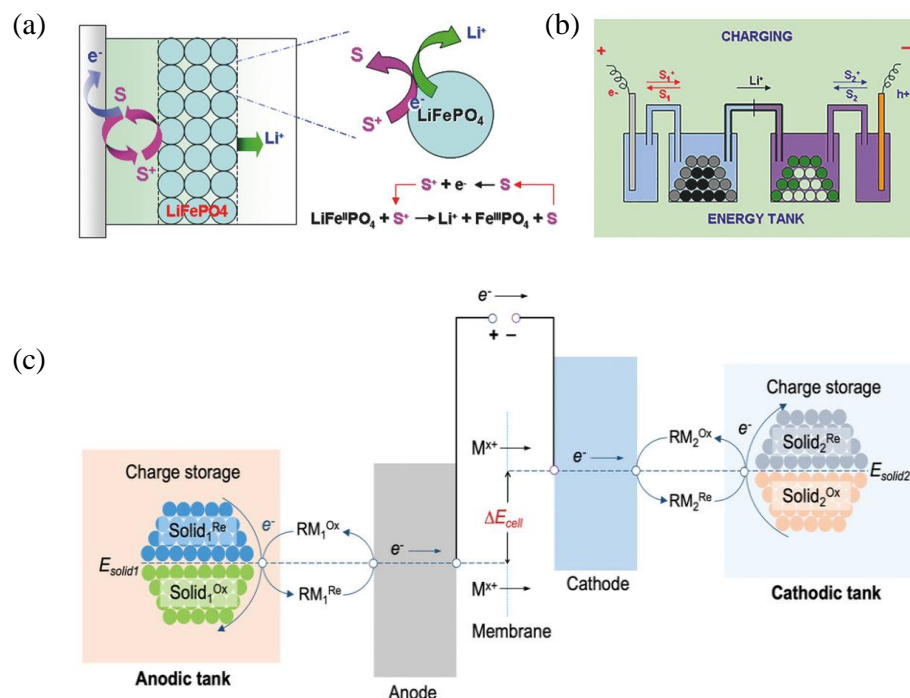


Figure 4. (a) RT reaction of battery material via freely diffusing RMs. (b) Illustration of an electric–energy–storage system. (c) Energy storage with an anodic tank and a cathodic tank. (a,b) and (c) are reprinted with permissions from references [30,36].

As shown in the Figure 4c, the RM undergoes electrochemical reactions on the electrode, resulting in its oxidation or reduction. Subsequently, it enters into chemical reactions with the solid materials within the tank, eliminating the need for direct electrode contact [29]. Moreover, solid materials are often configured in a granular form due to the advantages of rapid charging rates and facilitating dense packing. The chemical reactions between the solid materials and RMs occur within the tank. Consequently, the design of the tank size directly impacts the utilization efficiency and reaction rate between them. Therefore, the tank needs to meet three essential requirements. First, the tank must ensure that tightly packed, jagged-shaped solid materials do not cause system clogging. Thus, necessitating specific spatial considerations. Second, it should facilitate thorough contact between RMs and the solid materials within, allowing chemical reactions to occur and ensuring the progress of the redox-targeting (RT) reaction. Lastly, and most importantly, the tank must ensure that the solid materials remain within it and does not enter the electrodes, as this would directly impact the battery’s lifespan. This process leads to the reduction or oxidation of the RM and, in parallel, the oxidation or reduction of the solid material. This cyclic sequence repeats, facilitating the integration of the RM–solid materials reaction and the reversible electrochemical reactions of the RM, enabling large-scale application. In theory, any redox-species displaying reversible characteristics, with a standard potential closely aligned with the Fermi level of the battery material, has the potential to be considered suitable for the RT reaction.

To increase energy density, three strategies can be employed: (1) increasing the battery voltage, (2) enhancing the actual concentration of RMs, and (3) achieving multiple redox processes [50]. Despite the potential for non-aqueous systems to offer higher cell voltage,

thereby increasing their energy density, it is worth noting that these systems tend to exhibit relatively lower ionic conductivity for organic electrolytes. In contrast, aqueous electrolyte systems, while yielding lower voltage due to hydrogen and oxygen evolution reactions, possess excellent ionic conductivity along with enhanced safety, economic viability, and environmental benefits [30]. Currently, the observed findings indicate that the majority of organic RMs exhibit only one- or two-electron processes. When three-electron transfer or more is involved, the solubility and stability of these organic RMs are significantly compromised [45,51]. Therefore, improving the solubility of RMs which undergo a reversible two-electron transfer reaction is an effective approach to enhance energy density [52]. In this regard, redox-targeting based AORFBs can avoid the aforementioned unfavorable reactions. Solid materials do not undergo reactions on the electrode, which can be stored separately without affecting viscosity, and capacity is no longer limited by electrolyte concentration but by the solid materials in the tank. Additionally, solid materials do not require conductive additives because they participate in charge and discharge through chemical reactions rather than electrochemical reaction.

3.2. Two-Molecule RT Reaction

In the initial exposition of the RT reaction, it was a common practice to utilize two distinct RMs possessing appropriate potentials, which were paired with a single active solid material. This pairing was performed with the objective of facilitating two-way RT reactions. In 2013, Huang et al. proposed the pioneering redox-flow lithium battery (RFLB), which was a cathodic half-cell. This innovation operated within the cathodic tank, utilizing LiFePO_4 as the solid material, ferrocene, and 1,1'-dibromoferrocene as the RMs in the catholyte [53]. The feasibility of RFLB was substantiated through experimental results and various characterization techniques, which provided conclusive evidence of the occurrence of redox-targeting in the system. In 2014, Pan et al. constructed an assembly of an anodic half-cell of RFLB with CoCp_2 and CoCp^*_2 as RMs and using TiO_2 as the solid materials [54]. By combining the cathodic RFLB half-cell with this component, one can envision the creation of a complete RFLB full-cell. Which was demonstrated in 2015 utilizing the aforementioned solid materials and RMs (Figure 5a) [55]. During the charging process, Figure 5c shows three consecutive plateaus. The first one corresponds to the oxidation of Fc, and the simultaneous reduction of $\text{Co}(\text{Cp})_2^+$. $\text{Co}(\text{Cp}^*)_2^+$ is reduced after the reduction of $\text{Co}(\text{Cp})_2^+$ desists. Simultaneously, Fc perpetually undergoes oxidation, likely owing to the higher reaction reversibility of Fc, resulting in the second one, as illustrated in Figure 5b. Once Fc^+ is completely consumed, FcBr_2 starts to undergo oxidation, leading to the third one. The energy density of the cell could potentially reach a higher energy density, marking a tenfold increase compared to that of a VRFB.

Fan et al. showed the operation of lithium polysulfide cells in both continuous and intermittent flow modes unprecedentedly [56]. However, excessive conductive additives can increase viscosity, reducing energy storage capacity. Moreover, as the concentration of RM increases, the physical and electrochemical properties of RM may deteriorate. In order to tackle the mentioned challenges, Li et al. implemented the "redox-targeting" concept in such flow batteries, which utilized two RMs, CrCp^*_2 and NiCp^*_2 with high stability to achieve the reversible lithiation/delithiation of $\text{S}/\text{Li}_2\text{S}$ (Figure 5d) [57]. By incorporating solid materials in addition to the redox species, Figure 5e shows that an impressive nearly eightfold increase in capacity was achieved. Furthermore, this battery can operate effectively even with completely insulating $\text{S}/\text{Li}_2\text{S}$ materials, allowing for the elimination of approximately 30% of conductivity additives. This elimination of conductivity additives has the potential to significantly enhance the energy density. Moreover, this approach circumvents the need to pump a viscous fluid or slurry containing suspended solids, thereby mitigating challenges associated with high energy consumption.

Recently, Hatakeyama-Sato et al. presented 4 V-class organic polymer RMs that incorporate thianthrene derivatives, which exhibit higher potentials compared to conventional organic RMs [58]. This increased potential allows for the charging of LiMn_2O_4 , with a

significant theoretical capacity of 500 Ah/L. The design of soluble or nanoparticle polymers proves useful in mitigating the crossover, with only approximately 3% observed after 12 days of testing, while also contributing to mediating reactions. By developing thianthrene-based RMs with distinct molecular geometries, including small molecules, they also found that the polymeric materials with larger molecular radii had a positive impact on mitigating undesired crossover reactions, even porous separators. These findings hold the promise of advancing the development of flow cells with an organic/inorganic hybrid design, resulting in flow cells that offer higher energy density and extended lifespan. The design of this polymer is aimed at preventing quick permeability. The reason is that the monomer molecules have a small diameter, which leads to rapid penetration. The polymer does not affect the redox potential. However, a drawback is that the solubility of the polymer is low, causing an RT reaction to occur between solid materials and particles. This leads to a reduction in diffusion rate and a decrease in the contact area between them.

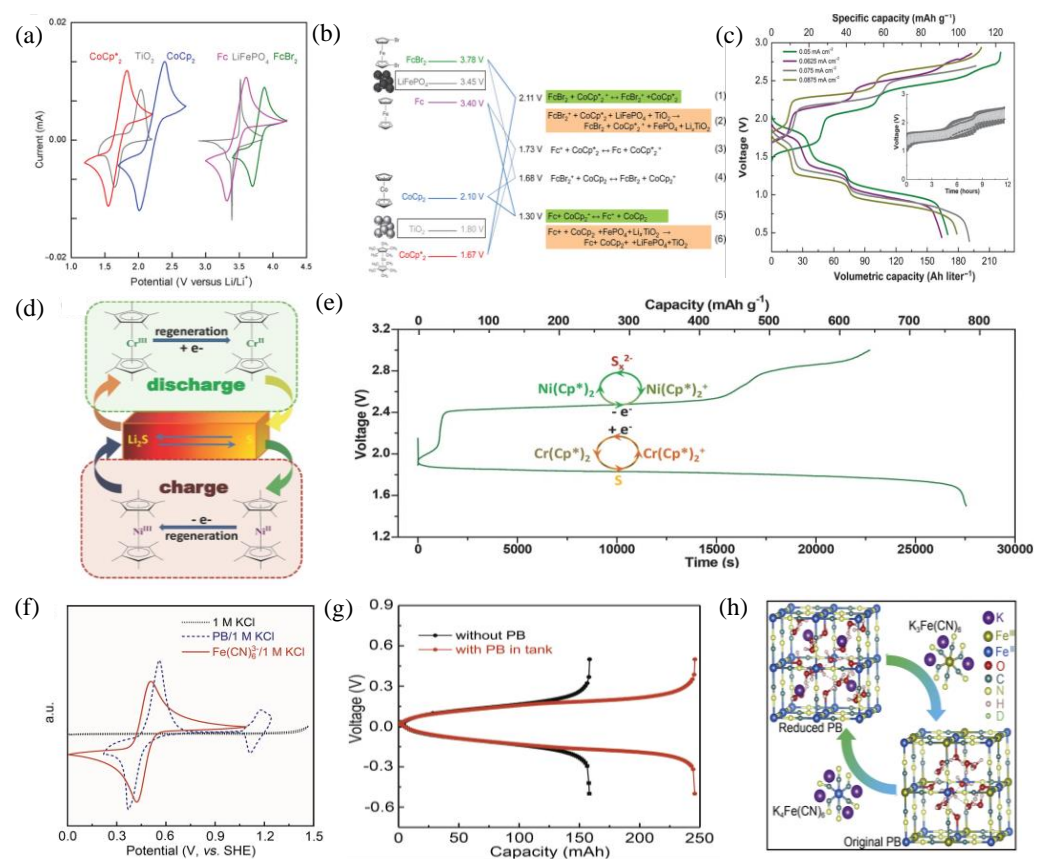


Figure 5. (a) CVs of the RMs, LiFePO_4 and TiO_2 . (b) A comprehensive depiction of the chemical interactions among the RMs and the substances contained within the tanks. (c) Voltage profiles at varying current densities. (d) A depiction of the redox reactions of lithium polysulfide cells. (e) Discharge/charge curves of a RFB with the addition of poly(S-r-DIB). (f) CVs of PB and $[\text{Fe}(\text{CN})_6]^{3-}$. (g) Voltage versus capacity with or without PB in tank at 20 mA cm⁻². (h) The most probable configurations of original and reduced PB. (a–c), (d,e), (f–h) are reprinted with permissions from references [55,58,59].

3.3. Single-Molecule RT Reaction

Nonetheless, the two-molecule RT reaction typically results in a voltage decline due to the relatively substantial disparity in their potentials. Furthermore, during a comprehensive cell demonstration, the two-molecule system encompasses the involvement of four distinct RMs and undergoes a total of four successive stages of reactions. This intricate setup introduces significant operational complexity and adversely impacts the cycling

stability of the battery [60]. To mitigate these concerns, Zhou et al. first introduced the concept of single-molecule redox-targeting (SMRT) instead of two RMs, which resulted in the attainment of a remarkable 95% voltage efficiency with the molecule (1-Ferrocenylmethyl-3-methylimidazolium bis (trifluoromethanesulfonyl) amide, FcIL) [61]. This achievement also led to a considerable upsurge in energy density to 330 Wh/L without compromising the essential characteristics of RT-AORFBs and simplifies the composition of the electrolyte. The reaction between RM and the solid materials relies solely on the Nernstian potential difference, which makes the voltage profile demonstrate a single charge/discharge plateau, effectively eradicating voltage hysteresis and thereby significantly enhancing voltage efficiency.

In 2018, Yu et al. employed $[\text{Fe}(\text{CN})_6]^{4-}/[\text{Fe}(\text{CN})_6]^{3-}$ and $\text{S}^{2-}/\text{S}_2^{2-}$ as RMs in the catholyte and anolyte. The cell achieved an impressive volumetric capacity [25]. Upon loading LiFePO_4 and $\text{LiTi}_2(\text{PO}_4)_3$ as the solid materials into the cathode and anode sides, it attained an anodic capacity of 305 Ah/L and a cathodic capacity of 207 Ah/L, which outperformed the VRFB, exhibiting a 4- to 6-fold improvement. Chen et al. employed Prussian blue ($\text{Fe}_4[\text{Fe}(\text{CN})_6]_3$, PB) as a cost-effective and robust capacity-enhancing material for utilization in neutral aqueous RFBs in 2019 [62]. The introduction of PB as a solid material in the system, coupled with its chemical reactions with $[\text{Fe}(\text{CN})_6]^{4-/3-}$, has effectively overcome the solubility limitations. This breakthrough has significantly enhanced the electrolyte's capacity. Compared to other $[\text{Fe}(\text{CN})_6]^{4-/3-}$ systems, this electrolyte configuration has achieved an unprecedented volumetric capacity of 61.6 Ah/L, setting a remarkable record. Moreover, Figure 5f shows that PB displays two reversible redox reactions occurring at 0.25 V and 0.92 V under neutral conditions, and closely mirrors the potentials of $[\text{Fe}(\text{CN})_6]^{4-/3-}$ and Br^-/Br_2 , respectively. This allows PB to be employed as a solid material in both the anode and cathode, with $[\text{Fe}(\text{CN})_6]^{3-}-\text{Br}^-$ serving as the redox pair. Furthermore, the system achieved PB utilization exceeding 50% at 20 mA/cm², while maintaining an exceptional capacity retention rate of over 99.991% per cycle during continuous testing. Upon the introduction of PB granules with roughly equal capacity, the discharge capacity witnessed a rise to 245.5 mAh, indicating the utilization of the solid materials amounting to 54.7% (Figure 5g). While anion-exchange membranes can be also used in neutral electrolytes, their conductivity and durability are far inferior to cation-exchange membranes. Moreover, with the use of cation-exchange membranes, the crossover between $[\text{Fe}(\text{CN})_6]^{4-/3-}$ and Br^- was mitigated which made Coulombic efficiency remarkable. Therefore, the choice of the membrane is crucial. Selecting the appropriate membrane allows specific ions to pass through while blocking unwanted substances, and it must also withstand corrosion. Hence, ion-exchange membranes play a pivotal role in flow batteries, directly impacting the battery's performance, efficiency, lifespan, and stability. With such numerous advantages, this system holds great prospects. Figure 5h shows the structure of PB, specifically one $\text{Fe}(\text{II})(\text{CN})_6$ vacancy that contains six coordinated H_2O molecules bonded to $\text{Fe}(\text{III})$ at empty nitrogen sites. Surrounding this vacancy, there are eight uncoordinated H_2O molecules, which is in accordance with the proposed structure for the insoluble properties of PB [59].

In the wake of the PB-based SMRT reaction, Cheng et al. addressed the challenges associated with conventional VRFBs, including low energy density, a limited operating temperature range, and high production costs, by proposing an RT-based VRFB system (RT-VRB) [63]. This system incorporates a Prussian blue analogue (PBA) as a capacity-enhancing component, enabling a reduction in catholyte concentration without compromising overall capacity. Consequently, this widens the temperature range of the RT-VRB compared to a standard VRFB. The theoretical volumetric capacity significantly surpasses that of a conventional VRFB, indicating potential for a substantial increase in energy storage capacity within the same volume. However, PBA presents superior reaction kinetics compared to PB, but the amount of vanadium in PBA has led to a significant increase in its cost. It is best to find an element to replace the expensive vanadium without affecting its redox potential and the increase in capacity.

4. Redox-Targeting Based RT Systems

4.1. Anthraquinone (AQ)-Based RT Systems

Conventional RFBs with inorganic species often employ transition metal ions under acidic condition. However, these systems encounter several obstacles, such as high material costs, crossover issues, and the use of corrosive or hazardous electrolytes, which impede their large-scale deployment. In contrast, the use of organic RMs abundant in nature has emerged as an appealing alternative to inorganic counterparts in RFBs [64]. Nonetheless, these systems still grapple with the persistent challenge of low solubility of RMs. To mitigate the low solubility issue of 9,10-anthraquinone-2,7-disulphonic acid (2,7-AQDS) under neutral conditions, Zhou et. al. employed the SMRT reaction, utilizing cost-effective polyimide as the solid material, which enhanced its capacity to 97 Ah/L (Figure 6a) [65]. Thanks to the structural similarity between polyimide and AQDS, as well as their identical redox potentials (Figure 6b), the energy density of the cell was improved to 39 Wh/L, with polyimide boosting the capacity of 2,7-AQDS in a neutral buffer solution by over eight times (Figure 6c). However, at a high current density, the voltage and energy efficiency of the system are not ideal. This is primarily due to an increase in internal resistance within the battery. Therefore, further optimization of the membrane is necessary.

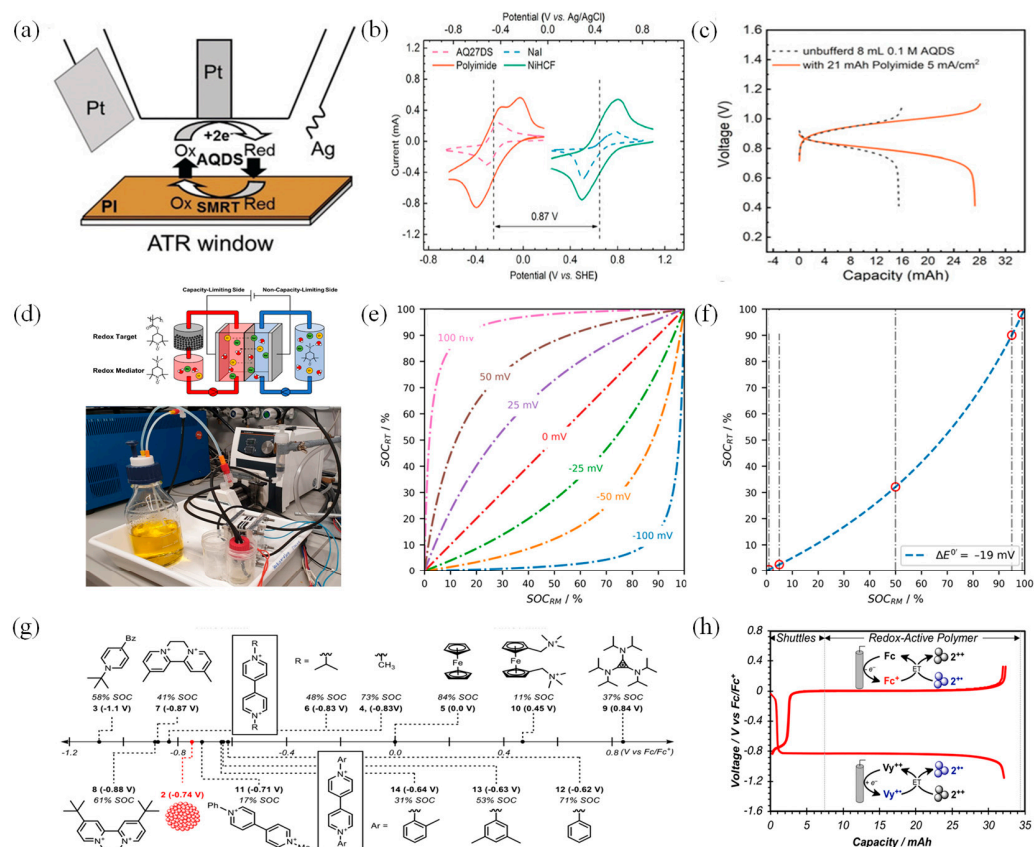


Figure 6. (a) In situ ATR–FTIR for the SMRT reaction between PI and AQDS. (b) CV curves of RMs and solid materials. (c) Voltage profiles with/without PI in unbuffered solutions at 5 mA cm⁻². (d) Illustration of a RFB comprising TMATEMPO and PTMA. (e) Calculated SOC_{RM} versus SOC_{RT} for distinct potential differences, $\Delta E_0'$, from -100 to +100 mV. (f) Calculated SOC_{RM} versus SOC_{RT} for the experimental value of $\Delta E_0' = -19$ mV. (g) $E_{1/2}$ vs. Fc/Fc⁺ for each RM. (h) Voltage profile versus capacity. (a–c), (d–f), and (g,h) are reprinted with permissions from references [61,66,67].

Subsequently, Huang et al. presented an AORFB that demonstrates a consistent battery capacity of approximately 573 mAh, by integrating a 1,5-dihydroxyanthraquinone (1,5-DHAQ)/poly (anthraquinonyl sulfide) anolyte with a [Fe(CN)₆]^{3-/4-} catholyte [66].

Additionally, it maintains an average voltage of around 0.89 V. The degradation of DHAQ can be ascribed to the breaking and formation of hydrogen bonds between the reduced form of anthraquinone and water. In contrast, 1,5-DHAQ has been found to possess a pronounced hydrogen bond structure, which makes the molecule stable during reduction. In the absence of solid materials, most of the 1,5-DHAQ undergoes reduction, triggering side reactions. Hence, PAQS serves as a buffer, enabling the reduced state of 1,5-DHAQ to account for half of the proportion, thereby stabilizing the anolyte system.

4.2. TEMPO-Based RT Systems

Schröter et al. presented the first investigation of a fully organic Nernstian potential-driven RT system, comprised of poly (TEMPO-methacrylate) (PTMA) as the solid materials and N,N,N-2,2,6,6-heptamethylpiperidinyloxy-4-ammonium chloride (TMATEMPO) as the single RM, which reached a capacity utilization of 78% of solid materials (Figure 6d) [60]. After the addition of PTMA, the capacity of the battery increased from 3.7 mAh to 11.4 mAh. However, originally, PTMA was hydrophobic, but as the cycling progressed, it gradually became hydrophilic. This change also led to material swelling, resulting in increased internal pressure and consequently, electrolyte leakage. For the PTMA/TMATEMPO system, the increasing pressure by the PTMA swelling resulted in recurrent cell failures around the 50-cycle mark due to electrolyte leakage. Such expansion not only reduces the battery's capacity but also renders its volume and porosity unmeasurable. Consequently, rendering volumetric capacities unquantifiable. Therefore, TEMPO-based ORFBs still require further research efforts to address and improve the issue of material expansion. Despite the limitations mentioned, it showcased the potential of the all-organic RT approach and proposed future strategies to address the capacity and cyclability constraints. These strategies encompass enhancing the concentration of RMs, augmenting the interfacial area between RM and solid material, improving the hydrophilicity of the solid material, and enhancing the chemical compositions of RM and solid material, which will enhance the energy density and cycle-life of RT systems.

Figure 6e,f demonstrates the relationship between SOC_{RT} and SOC_{RM} and $\Delta E^{0'}$, between the RM and RT (Equation (2)). The SOC increases during charging, while the SOC_{RT} remains unchanged as it remains stationary. However, when the charged RM encounters the uncharged RT, the charge from RM transfers to RT, eventually equalizing the potential difference (Equation (3)). The opposite process occurs during discharge. A larger $|\Delta E^{0'}|$ makes it more challenging to accurately determine the complete capacity of the RT. Hence, the optimal condition for RT reaction is achieved when $\Delta E^{0'}$ approaches zero. The equations above are as follows [60]. In the equation, $\Delta E^{0'}$ represents the potential difference between the redox reactions of RM and RT. R denotes the universal gas constant, T represents the temperature, z represents the number of transferred electrons, and F represents Faraday's constant.

$$SOC_{RT} = \left[1 + \exp \left(\frac{zF}{RT} \Delta E - \frac{zF}{RT} \Delta E^{0'} \right) \frac{1 - SOC_{RM}}{SOC_{RM}} \right]^{-1} \quad (2)$$

$$SOC_{RT} = \left[1 + \exp \left(-\frac{zF}{RT} \Delta E^{0'} \right) \frac{1 - SOC_{RM}}{SOC_{RM}} \right]^{-1} \quad (3)$$

4.3. Ferrocene-Based RT Systems

In 2020, Yu et al. utilized Fc-SO₃Na, a sulfonated ferrocene derivative, as the cathodic RMs and zinc metal as the anode, which was designed for pH-neutral aqueous RFBs [68]. Fc-SO₃Na boasts high water solubility and demonstrates impressive electrochemical reversibility and stability. This battery exhibits noteworthy characteristics at low concentration, including a capacity retention rate of 99.9975% per cycle. At higher concentrations it achieves an energy density of 27.1 Wh/L, which is competitively comparable to conventional VRFBs ranging from 25 to 30 Wh/L. Additionally, the introduction

of LiFePO_4 as a solid material into the cathodic tank led to a RT reaction with $\text{Fc-SO}_3\text{Na}$ and $\text{BrFc-SO}_3\text{Na}$. This resulted in a substantial increase in volumetric capacity, reaching 293.5 Ah/L, assuming that the porosity of LiFePO_4 is 50%. Considering additional advantages such as excellent cycling stability, an eco-friendly pH-neutral supporting electrolyte, and the abundance of resources for the RMs and LiFePO_4 as the solid material, the RFB system holds tremendous potential for large-scale applications. After extended cycling, there has been a slight decline in the battery capacity attributed to the degradation of the zinc electrode as well as the occurrence of dendritic growth where metallic zinc tends to penetrate the membrane [69].

4.4. Viologen-Based RT Systems

The preceding three organic species categories all operate under aqueous conditions, and it is worth noting that non-aqueous organic RT reactions based on viologen are also promising [70]. Viologen, an anolyte, has gained widespread recognition in the fields of electrochemistry, primarily because of its stable $2+/1+$ redox couple. Its counterparts have been extensively investigated as small molecules [71,72], oligomers, or polymers, making them suitable for massive energy storage applications in both aqueous and non-aqueous environments. When it comes to RT-based flow battery (RTFB) applications, despite the initially promising nature of solid materials in granular form due to their high charge rates and accessible SOC, they caused issues like high backpressure and system clogging due to their tightly packed jagged shapes. To overcome these problems and maintain charging performance, Wong and Sevov synthesized spherical solid materials with polystyrene derivatives of viologen in a range of sizes through minor variations to water, benzene, and surfactant [67]. As illustrated in Figure 6g, they highlighted the significance of the shuttle's structural properties in determining the discharge rate and depth of the redox-active polymer (RAP) while the electronic properties play a minimal role. It emphasizes the importance of designing shuttles with appropriate molecular structures rather than extreme oxidizing or reducing properties. The addition of solid materials significantly boosted storage capacity, increasing it by a factor of four, which aligned with over 90% utilization of the solid materials (Figure 6h). This indicates that choosing suitable sizes for RT particles can potentially mitigate clogging issues. Due to the lack of a clear comprehension of the connection between electron transfer rates and yields in solid materials and RMs, Wong and Sevov also devised a novel technique to indirectly assess the redox changes in the solid materials by using CV. Guided by this analytical approach, they engineered modified RMs that effectively charged the solid materials to high SOCs, achieving excellent electrochemical performance in the RT-AORFBs' system.

4.5. Advanced Characterization Methods

Characterization methods are vital for understanding redox-active material properties and their operational and degradation mechanisms in RFBs. To formulate effective guidelines for designing RMs for RFBs, it is imperative to have a profound grasp of reaction mechanisms and cycling stability. Spectroscopic techniques, like ultraviolet and visible spectrophotometry (UV-Vis), X-ray photoelectron spectroscopy (XPS), X-ray diffraction (XRD) and electron paramagnetic resonance (EPR) spectroscopy, are preferred for studying RT reactions in the liquid electrolytes.

To monitor the changes in valence states of $\text{Na}_3\text{V}_2(\text{PO}_4)_3$ (NVP) in the cathode side, as well as the corresponding evolution of MPTZ concentration in real-time, operando X-ray absorption near edge structure (XANES) spectroscopy was employed to examine SMRT reaction [73]. This technique is widely used to investigate variations in valence states and chemical environments in battery materials. When the SOC reached 60% for the mediators in the catholyte, there was minimal change in absorption. This suggests that the mediator is not effectively oxidizing NVP in this range, and the capacity is primarily contributed by MPTZ to MPTZ^+ . However, when the SOC reached 65%, reaching a thermodynamic driving force threshold, the absorption edge of vanadium (V) rapidly moves in the direction

of higher energy. This shift indicates significant changes in the valence state of V during the SMRT reaction. Notably, isobestic points were observed at approximately 5495, 5518, and 5560 eV, indicating phase transitions of NVP with MPTZ^+ during SMRT reaction (Figure 7a). These observations provide insights into the dynamic changes occurring in the system during the SMRT reaction and highlight the role of MPTZ^+ in the redox processes.

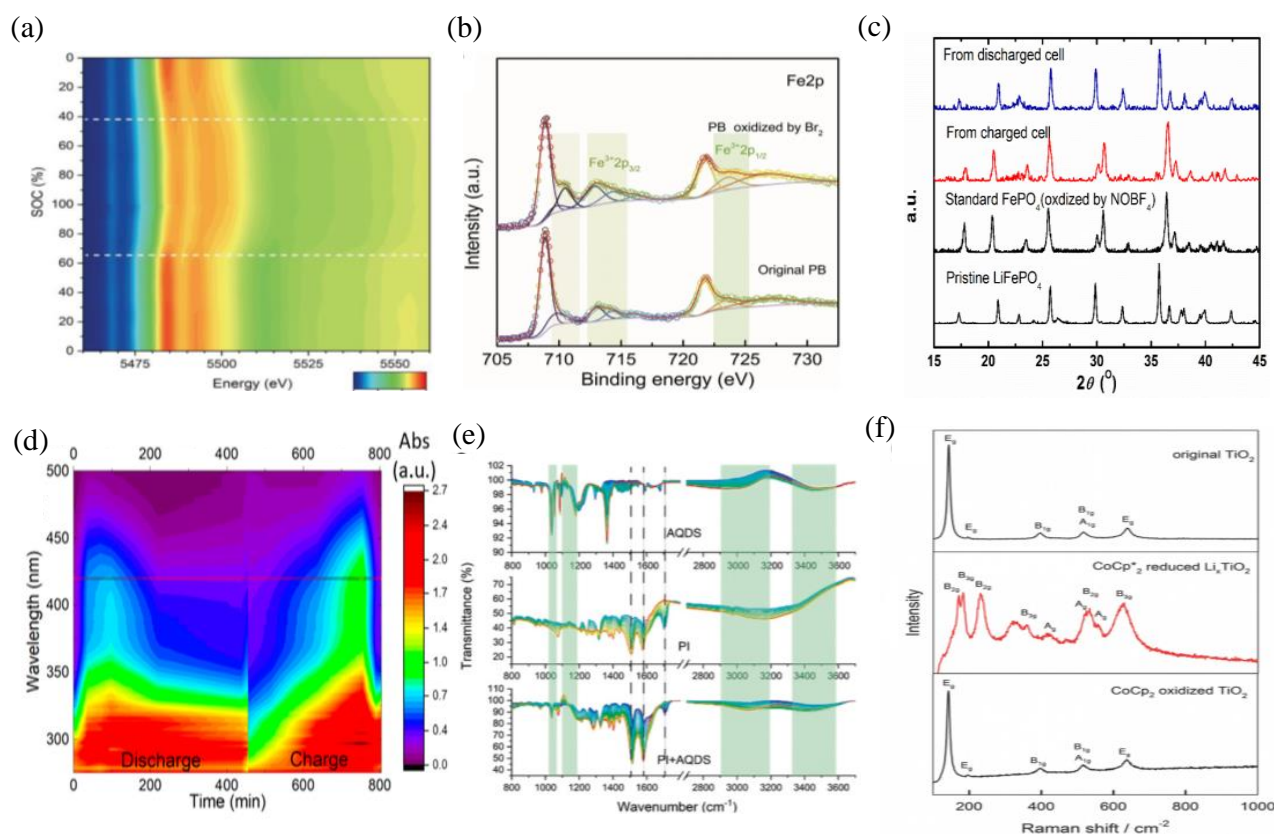


Figure 7. (a) Operando X-ray near edge absorption of V K-edge at 0.45 mA cm^{-2} . (b) Fe 2p XPS spectra of PB and Br_2 -oxidized PB. (c) Ex-situ XRD patterns of the solid materials and the comparison with the standard LiFePO_4 and FePO_4 . (d) Alteration in the absorbance at 420 nm within UV-vis spectra (e) Comparison of AQDS, PI and AQDS + PI spectra. (f) Raman spectra of anatase TiO_2 . From the top down, original, lithiated, and re-delithiated states, respectively. (a), (b), (c), (d), (e) and (f) are reprinted with permissions from references [55,61,62,66,73,74].

Chen et al. utilized XPS to confirm the SMRT reaction [62]. In addition to the reversible reaction of PB/PW, PB undergoes another one at an elevated redox potential (0.92 V, compared to Ag/AgCl), involving the transformation of PB and BG. It has been observed that PB can undergo oxidation through Br_2 , which is supported by XPS measurements (Figure 7b). The Fe (III) in the Fe 2p spectra significantly heightens following its reaction with Br_2 . Furthermore, Br^- has the capability to reduce BG back to PB. In addition, ex situ XRD was used to investigate the phase transformation of solid materials (Figure 7c). Zhou et al. utilized XRD to observe that LiFePO_4 undergoes nearly full conversion into FePO_4 during the charging process and subsequently returns to its original LiFePO_4 structure upon discharging [61]. This finding provides strong supporting evidence for RT reaction involving FcIL with LiFePO_4 which entails a process of lithiation and delithiation.

UV-vis spectroscopy is carried out to detect changes in absorbance at specific wavelengths, which can provide information about the chemical changes occurring in a system. Meyerson et al. utilized UV-vis to demonstrate the occurrence of redox-targeting reaction [74]. During discharge, elemental S undergoes an initial conversion into higher-order polysulfides (PSs) which subsequently transition into lower-order PSs and ultimately, trans-

form into lithium sulfide (Li_2S). Figure 7d displays a contour plot of the UV–vis spectra depicting variations in absorbance. The concentration of PSs increases at the start of discharge, subsequently declining towards the end of the discharge phase as it transforms into Li_2S . Although Li_2S is not directly visible in UV-Vis, the reduction in all PSs species strongly implies their conversion into Li_2S . Attenuated total reflection (ATR)-FTIR is also an analytical technique used for real-time monitoring of chemical processes and reactions at a solid-liquid interface. To confirm the SMRT reaction and uncover its underlying mechanism, Zhou et al. utilized the in situ ATR-FTIR to detect real-time bonding information of both the RMs (2,7-AQDS) and the solid materials (PI) during CV scans [65]. An analysis of Figure 7e reveals that the C=O and C-O stretching bands at 1679 and 1364 cm^{-1} in the 2,7-AQDS/2,7-AQDS²⁻ spectra became indistinguishable in the PI + AQDS spectra. Conversely, the IR signals of AQDS in the fingerprint region (800–1200 cm^{-1}) and the O-H stretching vibration (2800–3800 cm^{-1}) were noticeably enhanced, suggesting AQDS adsorption on PI and their interaction. To substantiate the conclusions deduced from the FTIR characterization, simultaneous employment of density functional theory (DFT) calculations were employed to bolster the notion.

Moreover, they also used ex situ FTIR to confirm the RT reaction in the cathodic tank. In order to explore the RT reactions involving 1,5-DHAQ and PAQS/CB, Huang et al. employed operando FTIR to track the bonding changes in PAQS through multiple CV scans [66]. The appearance of the C–O bond stretching vibration in reduced PAQS at 1371 cm^{-1} during 1,5-DHAQ reduction and its disappearance upon 1,5DHAQ²⁻ oxidation were observed. Additionally, the reversible alterations in vibrations at 1303 and 1262 cm^{-1} , linked to aromatic ring vibrations between the neutral and ionized forms (PAQS²⁻), further substantiated the progression of the SMRT reactions. Pan et al. utilized CoCp^*_2 and CoCp_2 as RMs and TiO_2 as the solid materials for the RT reactions [54]. To demonstrate the occurrence of RT reaction, they employed Raman spectroscopy. In Figure 7f, pristine anatase TiO_2 exhibited five peaks. After reduction by CoCp^*_2 , a new set of peaks emerged, indicating the lithiation of TiO_2 into Li_xTiO_2 . Subsequently, the lithiated electrode was reoxidized by CoCp_2^+ , resulting in spectra identical to the original one, signifying the chemical oxidation of Li_xTiO_2 back to TiO_2 , which provides evidence for the RT reactions.

The EPR spectrum is obtained by measuring the sample's absorption and radiation of microwave radiation. Fang et al. employed EPR to investigate a 1 mM TPz-1 sample prepared through electrochemical methods [51]. The EPR spectrum reveals signals corresponding to the presence of free radical species in the sample. By analyzing the EPR spectrum, the redox mechanism of TPz-1 was determined, demonstrating the formation of a free-radical species during the charging process. This result further validates the hypothesis of TPz molecules possessing a six-electron redox-activity, making TPz a promising anode material for alkaline RFBs. However, TPz has a low diffusion coefficient and poor battery performance. The subsequent investigation can focus on studying more stable derivatives of TPz with an aim to increase their diffusion coefficient without compromising the redox-activity.

5. Challenges and Outlooks

As mentioned above, the RT-AORFBs' system effectively addresses the issue of low solubility, leading to substantial enhancements in capacity, energy density, and excellent cycling stability. Furthermore, the characterization of the RT reaction is being developed, which further reveals the mechanism behind the RT reaction. This advancement enables a better understanding and utilization of the reaction for achieving higher capacity enhancements. However, there are still challenges to be addressed to achieve large-scale application:

Firstly, the stability of organic materials during battery cycling and the cyclic stability of solid materials and RMs are of paramount importance for various energy applications. Their stability significantly affects the lifespan of the battery. Both components undergo repetitive reactions, especially for RMs. Besides, solid materials used in RT-AORFBs must

remain entirely insoluble throughout all charge states to ensure they remain contained within the storage chambers. Any level of dissolution of the solid materials could lead to deposition within the tubing or electrolysis cell. Potentially causing blockages in the RT-AORFBs' system. Moreover, due to the strict requirements of the RT reaction in terms of potential matching and similarity in chemical structure, the options for SMRT systems are relatively limited as only one RM can be paired with solid materials. The larger the potential difference between the two, the less pronounced the RT reaction becomes, resulting in reduced capacity utilization of the solid materials. To address this issue, designing new RMs is a promising approach, leveraging the tunable properties of organic mediators. In the RT-AORFBs' system, the solubility of the RM is not the primary concern since the ultimate battery capacity relies on the capacity of solid materials. However, the stability and redox potential of the RM are crucial as they determine if the RT reaction can occur. Furthermore, high-throughput computations can be employed to design organic species and calculate their redox-potential's solubility. This greatly saves time spent on experimental exploration. Followed by advanced characterization techniques to verify their consistency with the computational results.

Secondly, the energy storage tank is essential for the RT-AORFBs' system, where the movement of redox species and their interactions with solid materials are crucial. Therefore, optimizing the reactor's design is crucial for better energy and power density, efficient material use, reliable cycling, and reduced maintenance, especially when in large-scale application. The energy density achievable in the tank is contingent upon the solid pellet loading, while the remaining space serves to accommodate volume fluctuations in materials during the charge/discharge processes. During the flow of RMs, excessive loading of solid materials may result in significant flow resistance. Therefore, the choice of the appropriate shape and size of solid materials is also crucial. Moreover, the validation of RT reaction between solid materials and RMs sharing the same redox moiety necessitates the careful selection of suitable solid materials and the use of low RM concentrations. The utilization of high RM concentrations would have made it more challenging to detect the redox-targeting reaction. The concerns mentioned above can be effectively tackled through the utilization of computer modeling. This valuable tool can proficiently forecast various aspects, including the chemical reaction process and fluid dynamics. This encompasses factors such as edge effects, flow distribution, and velocity contours.

Thirdly, the selection and optimization of membranes become a critical concern, as crossover through the standard separator becomes problematic during extended cycle times (>12 h) in these high-capacity cells. To make RT-AORFBs widely used, it is imperative to address the crossover issue associated with long cycling times. Currently, the most extensively utilized membranes are Nafion membranes. Nevertheless, the elevated costs associated with active redox couples and membranes significantly increase the capital expenditure of certain RFB systems, which account for approximately 30% to 40% of the total cost, further exacerbating the overall financial burden. Therefore, membrane optimization is crucial for the practical implementation of RT-AORFBs.

Last but not the least, the selection of electrolyte is crucial as it directly impacts the ionic conductivity of the solution. For large-scale applications, it is preferable to choose non-toxic and eco-friendly electrolytes. Additionally, the solubility and reaction kinetics of the RM are influenced by the surrounding solvation environment which can be modulated by different electrolytes. The choice of electrolyte can yield diverse solubility profiles and reaction kinetics for various RMs. For example, the addition of the buffer solution (NaAc + HAc) not only increased the solubility of the reduced state of AQDS but also facilitated the entire SMRT reaction. Therefore, it is important to find the most suitable electrolyte for each specific RM. Furthermore, for some organic species, which involve proton-coupled electron transfer (PCET) redox reactions, the pH can affect their redox potentials. For example, quinones. Hence, studying how the redox potential changes with pH for such species is crucial. This will be helpful for matching the redox potential of the RM with the energy storage material and preventing hydrogen and oxygen evolution reactions.

6. Conclusions

This review delves into the recent advancements in all-organic RT redox flow batteries, transitioning from the initial focus on bimolecular RT reactions to single-molecule reactions. In addition to highlighting the drawbacks of current RFBs, we also present a comprehensive introduction and summary of the concept, advantages, and critical materials employed in the development of RT-AORFBs. The article discusses the application of RT reaction in various types of systems, and all of them have led to an improvement in battery energy density, indicating its broad applicability. Among the various types, we believe an all-organic aqueous RT system holds the most promising sustainable outlook. Primarily due to its low cost, abundant materials, and high safety level. However, it is necessary to point out the limitations before its widespread implementation, such as the stability of RMs and solid materials, design of storage tanks, optimization of membranes, and crucial selection of electrolytes, especially for organic aqueous systems. By addressing these challenges, we firmly believe that an all-organic aqueous RT system holds tremendous potential for large-scale sustainable energy storage and can become the preferred choice in the future.

Author Contributions: Conceptualization, J.M. and Y.J.; validation, J.M., S.R., Z.H. and T.W.; writing—original draft, J.M.; chart analysis, J.M., S.R. and Y.C.; data curation, J.M., Y.C. and T.W.; supervision, Y.J.; project administration, Y.J. All authors have read and agreed to the published version of the manuscript.

Funding: This work was supported by the Shanghai Sailing Program (BI2800006) and the SJTU-Warwick Joint Seed Fund (WH610160507/053).

Conflicts of Interest: The authors declare no conflict of interest.

Abbreviations

Abbreviation	Meaning
AORFBs	Aqueous organic redox flow batteries
RT	Redox-targeting
PSH	Pumped-storage hydropower
RFB	Redox flow battery
VRFBs	Vanadium redox flow batteries
RMs	Redox mediators
solid materials	Energy storage solid materials
RT-AORFBs	Redox-targeting aqueous organic redox flow batteries
AQ	Anthraquinones
OCV	Open-circuit voltage
SOC	State of charge
2,6-DHAQ	2,6-dihydroxyanthraquinone
PEG	Polyethylene glycol
RFLB	Redox-Flow Lithium Battery
TEMPO	(2,2,6,6-tetramethylpiperidin-1-yl) oxyl
MV	Methyl viologen
SMRT	Single-Molecule Redox-Targeting
RT-VRB	a RT-based VRFB system
PBA	Prussian blue analogue
2,7-AQDS	9,10-Anthraquinone-2,7-disulphonic acid
1,5-DHAQ	1,5-Dihydroxyanthraquinone
PTMA	Poly (TEMPO-methacrylate)
RTFB	RT-based flow battery
RAP	Redox-active polymer
UV-Vis	Ultraviolet and visible spectrophotometry
XPS	X-ray photoelectron spectroscopy
XRD	X-ray Diffraction
2,6 DAEAQ	N,N-(9,10-anthraquinone 2,6-diyl)-di- β -alanine
EPR	Electron Paramagnetic Resonance

XANES	X-ray absorption near edge structure
PSs	Polysulfides
ATR	Attenuated total reflection
DFT	Density Functional Theory
TEMPTMA	N,N,N-2,2,6,6-heptamethyl piperidinyl oxy-4-ammonium chloride
PCET	Proton-coupled electron transfer

References

- Dresselhaus, M.S.; Thomas, I.L. Alternative Energy Technologies. *Nature* **2001**, *414*, 332–337. [[CrossRef](#)]
- Weber, A.Z.; Mench, M.M.; Meyers, J.P.; Ross, P.N.; Gostick, J.T.; Liu, Q. Redox Flow Batteries: A Review. *J. Appl. Electrochem.* **2011**, *41*, 1137–1164. [[CrossRef](#)]
- Leung, P.; Li, X.; de León, C.P.; Berlouis, L.; Low, C.T.J.; Walsh, F.C. Progress in Redox Flow Batteries, Remaining Challenges and Their Applications in Energy Storage. *RSC Adv.* **2012**, *2*, 10125–10156. [[CrossRef](#)]
- Wang, Z.; Tam, L.-Y.S.; Lu, Y.-C. Flexible Solid Flow Electrodes for High-Energy Scalable Energy Storage. *Joule* **2019**, *3*, 1677–1688. [[CrossRef](#)]
- Wang, W.; Luo, Q.; Li, B.; Wei, X.; Li, L.; Yang, Z. Recent Progress in Redox Flow Battery Research and Development. *Adv. Funct. Mater.* **2013**, *23*, 970–986. [[CrossRef](#)]
- Noack, J.; Roznyatovskaya, N.; Herr, T.; Fischer, P. The Chemistry of Redox-Flow Batteries. *Angew. Chem. Int. Ed.* **2015**, *54*, 9776–9809. [[CrossRef](#)] [[PubMed](#)]
- Zheng, J.; Liu, X.; Li, W.; Li, W.; Feng, X.; Chen, W. Green Synthesis of Novel Conjugated Poly(Perylene Diimide) as Cathode with Stable Sodium Storage. *Nano Res.* **2023**, *16*, 9538–9545. [[CrossRef](#)]
- Lindley, D. Smart Grids: The Energy Storage Problem. *Nature* **2010**, *463*, 18–20. [[CrossRef](#)] [[PubMed](#)]
- Kwon, G.; Lee, S.; Hwang, J.; Shim, H.-S.; Lee, B.; Lee, M.H.; Ko, Y.; Jung, S.-K.; Ku, K.; Hong, J.; et al. Multi-Redox Molecule for High-Energy Redox Flow Batteries. *Joule* **2018**, *2*, 1771–1782. [[CrossRef](#)]
- Mao, J.; Ruan, W.; Chen, Q. Understanding the Aqueous Solubility of Anthraquinone Sulfonate Salts: The Quest for High Capacity Electrolytes of Redox Flow Batteries. *J. Electrochem. Soc.* **2020**, *167*, 070522. [[CrossRef](#)]
- Larcher, D.; Tarascon, J.-M. Towards Greener and More Sustainable Batteries for Electrical Energy Storage. *Nat. Chem.* **2015**, *7*, 19–29. [[CrossRef](#)] [[PubMed](#)]
- Long, Y.; Xu, Z.; Wang, G.; Xu, H.; Yang, M.; Ding, M.; Yuan, D.; Yan, C.; Sun, Q.; Liu, M.; et al. A Neutral Polysulfide/Ferricyanide Redox Flow Battery. *iScience* **2021**, *24*, 103157. [[CrossRef](#)] [[PubMed](#)]
- Nakagawa, Y.; Tsujimura, S. Fabrication of an Organic Redox Capacitor with a Neutral Aqueous Electrolyte Solution. *Electrochemistry* **2021**, *89*, 317–322. [[CrossRef](#)]
- Mohammadi, T.; Chieng, S.C.; Skyllas Kazacos, M. Water Transport Study across Commercial Ion Exchange Membranes in the Vanadium Redox Flow Battery. *J. Membr. Sci.* **1997**, *133*, 151–159. [[CrossRef](#)]
- Soloveichik, G.L. Flow Batteries: Current Status and Trends. *Chem. Rev.* **2015**, *115*, 11533–11558. [[CrossRef](#)]
- Jing, Y.; Liang, Y.; Gheytni, S.; Yao, Y. A Quinone Anode for Lithium-Ion Batteries in Mild Aqueous Electrolytes. *ChemSusChem* **2020**, *13*, 2250–2255. [[CrossRef](#)] [[PubMed](#)]
- Li, X.; Zhang, H.; Mai, Z.; Zhang, H.; Vankelecom, I. Ion Exchange Membranes for Vanadium Redox Flow Battery (VRB) Applications. *Energy Environ. Sci.* **2011**, *4*, 1147–1160. [[CrossRef](#)]
- Wu, M.; Bahari, M.; Jing, Y.; Amini, K.; Fell, E.M.; George, T.Y.; Gordon, R.G.; Aziz, M.J. Highly Stable, Low Redox Potential Quinone for Aqueous Flow Batteries. *Batter. Supercaps* **2022**, *5*, e202200009. [[CrossRef](#)]
- Sum, E.; Rychcik, M.; Skyllas-kazacos, M. Investigation of the V(V)/V(IV) System for Use in the Positive Half-Cell of a Redox Battery. *J. Power Source* **1985**, *16*, 85–95. [[CrossRef](#)]
- Zeng, Y.K.; Zhao, T.S.; An, L.; Zhou, X.L.; Wei, L. A Comparative Study of All-Vanadium and Iron-Chromium Redox Flow Batteries for Large-Scale Energy Storage. *J. Power Source* **2015**, *300*, 438–443. [[CrossRef](#)]
- Wei, X.; Pan, W.; Duan, W.; Hollas, A.; Yang, Z.; Li, B.; Nie, Z.; Liu, J.; Reed, D.; Wang, W.; et al. Materials and Systems for Organic Redox Flow Batteries: Status and Challenges. *ACS Energy Lett.* **2017**, *2*, 2187–2204. [[CrossRef](#)]
- Lin, K.; Chen, Q.; Gerhardt, M.R.; Tong, L.; Kim, S.B.; Eisenach, L.; Valle, A.W.; Hardee, D.; Gordon, R.G.; Aziz, M.J.; et al. Alkaline Quinone Flow Battery. *Science* **2015**, *349*, 1529–1532. [[CrossRef](#)]
- Leung, P.; Shah, A.A.; Sanz, L.; Flox, C.; Morante, J.R.; Xu, Q.; Mohamed, M.R.; Ponce de León, C.; Walsh, F.C. Recent Developments in Organic Redox Flow Batteries: A Critical Review. *J. Power Source* **2017**, *360*, 243–283. [[CrossRef](#)]
- Xu, Y.; Wen, Y.-H.; Cheng, J.; Cao, G.-P.; Yang, Y.-S. A Study of Tiron in Aqueous Solutions for Redox Flow Battery Application. *Electrochim. Acta* **2010**, *55*, 715–720. [[CrossRef](#)]
- Yu, J.; Fan, L.; Yan, R.; Zhou, M.; Wang, Q. Redox Targeting-Based Aqueous Redox Flow Lithium Battery. *ACS Energy Lett.* **2018**, *3*, 2314–2320. [[CrossRef](#)]
- Yan, R.; Wang, Q. Redox-Targeting-Based Flow Batteries for Large-Scale Energy Storage. *Adv. Mater.* **2018**, *30*, 1802406. [[CrossRef](#)]
- Ye, J.; Xia, L.; Wu, C.; Ding, M.; Jia, C.; Wang, Q. Redox Targeting-Based Flow Batteries. *J. Phys. D Appl. Phys.* **2019**, *52*, 443001. [[CrossRef](#)]

28. Zhang, F.; Gao, M.; Huang, S.; Zhang, H.; Wang, X.; Liu, L.; Han, M.; Wang, Q. Redox Targeting of Energy Materials for Energy Storage and Conversion. *Adv. Mater.* **2022**, *34*, 2104562. [[CrossRef](#)]
29. Wang, Q.; Zakeeruddin, S.M.; Wang, D.; Exnar, I.; Grätzel, M. Redox Targeting of Insulating Electrode Materials: A New Approach to High-Energy-Density Batteries. *Angew. Chem. Int. Ed.* **2006**, *45*, 8197–8200. [[CrossRef](#)]
30. Ruan, W.; Mao, J.; Chen, Q. Redox Flow Batteries toward More Soluble Anthraquinone Derivatives. *Curr. Opin. Electrochem.* **2021**, *29*, 100748. [[CrossRef](#)]
31. Wang, C.; Yu, B.; Liu, Y.; Wang, H.; Zhang, Z.; Xie, C.; Li, X.; Zhang, H.; Jin, Z. N-Alkyl-Carboxylate-Functionalized Anthraquinone for Long-Cycling Aqueous Redox Flow Batteries. *Energy Storage Mater.* **2021**, *36*, 417–426. [[CrossRef](#)]
32. Huskinson, B.; Marshak, M.P.; Suh, C.; Er, S.; Gerhardt, M.R.; Galvin, C.J.; Chen, X.; Aspuru-Guzik, A.; Gordon, R.G.; Aziz, M.J. A Metal-Free Organic–Inorganic Aqueous Flow Battery. *Nature* **2014**, *505*, 195–198. [[CrossRef](#)] [[PubMed](#)]
33. Jin, S.; Jing, Y.; Kwabi, D.G.; Ji, Y.; Tong, L.; De Porcellinis, D.; Goulet, M.-A.; Pollack, D.A.; Gordon, R.G.; Aziz, M.J. A Water-Miscible Quinone Flow Battery with High Volumetric Capacity and Energy Density. *ACS Energy Lett.* **2019**, *4*, 1342–1348. [[CrossRef](#)]
34. Wei, X.; Xu, W.; Vijayakumar, M.; Cosimbescu, L.; Liu, T.; Sprenkle, V.; Wang, W. TEMPO-Based Catholyte for High-Energy Density Nonaqueous Redox Flow Batteries. *Adv. Mater.* **2014**, *26*, 7649–7653. [[CrossRef](#)]
35. Winsberg, J.; Janoschka, T.; Morgenstern, S.; Hagemann, T.; Muench, S.; Hauffman, G.; Gohy, J.-F.; Hager, M.D.; Schubert, U.S. Poly(TEMPO)/Zinc Hybrid-Flow Battery: A Novel, “Green”, High Voltage, and Safe Energy Storage System. *Adv. Mater.* **2016**, *28*, 2238–2243. [[CrossRef](#)]
36. Liu, T.; Wei, X.; Nie, Z.; Sprenkle, V.; Wang, W. A Total Organic Aqueous Redox Flow Battery Employing a Low Cost and Sustainable Methyl Viologen Anolyte and 4-HO-TEMPO Catholyte. *Adv. Energy Mater.* **2016**, *6*, 1501449. [[CrossRef](#)]
37. Orita, A.; Verde, M.G.; Sakai, M.; Meng, Y.S. The Impact of pH on Side Reactions for Aqueous Redox Flow Batteries Based on Nitroxyl Radical Compounds. *J. Power Source* **2016**, *321*, 126–134. [[CrossRef](#)]
38. Ma, X.; Zhang, H.; Xing, F. A Three-Dimensional Model for Negative Half Cell of the Vanadium Redox Flow Battery. *Electrochim. Acta* **2011**, *58*, 238–246. [[CrossRef](#)]
39. Ding, C.; Zhang, H.; Li, X.; Liu, T.; Xing, F. Vanadium Flow Battery for Energy Storage: Prospects and Challenges. *J. Phys. Chem. Lett.* **2013**, *4*, 1281–1294. [[CrossRef](#)] [[PubMed](#)]
40. Janoschka, T.; Martin, N.; Hager, M.D.; Schubert, U.S. An Aqueous Redox-Flow Battery with High Capacity and Power: The TEMPTMA/MV System. *Angew. Chem. Int. Ed.* **2016**, *55*, 14427–14430. [[CrossRef](#)]
41. Seo, N.-U.; Kim, K.; Yeo, J.; Kwak, S.J.; Kim, Y.; Kim, H.; Kim, M.S.; Choi, J.; Jung, Y.S.; Chae, J.; et al. Covalent Conjugation of a ‘Hydroxide-Philic’ Functional Group Achieving ‘Hydroxide-Phobic’ TEMPO with Superior Stability in All-Organic Aqueous Redox Flow Batteries. *J. Mater. Chem. A* **2023**, *11*, 18953–18963. [[CrossRef](#)]
42. Page, J.A.; Wilkinson, G. The Polarographic Chemistry of Ferrocene, Ruthenocene and the Metal Hydrocarbon Ions. *J. Am. Chem. Soc.* **1952**, *74*, 6149–6150. [[CrossRef](#)]
43. Pauson, P.L. Ferrocene Derivatives. Part I. The Direct Synthesis of Substituted Ferrocenes. *J. Am. Chem. Soc.* **1954**, *76*, 2187–2191. [[CrossRef](#)]
44. Beh, E.S.; De Porcellinis, D.; Gracia, R.L.; Xia, K.T.; Gordon, R.G.; Aziz, M.J. A Neutral pH Aqueous Organic–Organometallic Redox Flow Battery with Extremely High Capacity Retention. *ACS Energy Lett.* **2017**, *2*, 639–644. [[CrossRef](#)]
45. Huang, J.; Hu, S.; Yuan, X.; Xiang, Z.; Huang, M.; Wan, K.; Piao, J.; Fu, Z.; Liang, Z. Radical Stabilization of a Tripyridinium–Triazine Molecule Enables Reversible Storage of Multiple Electrons. *Angew. Chem. Int. Ed.* **2021**, *60*, 20921–20925. [[CrossRef](#)] [[PubMed](#)]
46. Zhao, Y.; Ding, Y.; Song, J.; Li, G.; Dong, G.; Goodenough, J.B.; Yu, G. Sustainable Electrical Energy Storage through the Ferrocene/Ferrocenium Redox Reaction in Aprotic Electrolyte. *Angew. Chem. Int. Ed.* **2014**, *53*, 11036–11040. [[CrossRef](#)] [[PubMed](#)]
47. Park, K.; Cho, J.H.; Shanmuganathan, K.; Song, J.; Peng, J.; Gobet, M.; Greenbaum, S.; Ellison, C.J.; Goodenough, J.B. New Battery Strategies with a Polymer/Al₂O₃ Separator. *J. Power Source* **2014**, *263*, 52–58. [[CrossRef](#)]
48. Hwang, B.; Park, M.-S.; Kim, K. Ferrocene and Cobaltocene Derivatives for Non-Aqueous Redox Flow Batteries. *ChemSusChem* **2015**, *8*, 310–314. [[CrossRef](#)] [[PubMed](#)]
49. Hu, B.; DeBruler, C.; Rhodes, Z.; Liu, T.L. Long-Cycling Aqueous Organic Redox Flow Battery (AORFB) toward Sustainable and Safe Energy Storage. *J. Am. Chem. Soc.* **2017**, *139*, 1207–1214. [[CrossRef](#)]
50. Cong, G.; Lu, Y.C. Strategies to Improve the Energy Density of Non-Aqueous Organic Redox Flow Batteries. *Acta Phys.* **2021**, *38*, 2106008. [[CrossRef](#)]
51. Fang, X.; Cavazos, A.T.; Li, Z.; Li, C.; Xie, J.; Wassall, S.R.; Zhang, L.; Wei, X. Six-Electron Organic Redoxmers for Aqueous Redox Flow Batteries. *Chem. Commun.* **2022**, *58*, 13226–13229. [[CrossRef](#)] [[PubMed](#)]
52. Material Design and Engineering of Next-Generation Flow-Battery Technologies | Nature Reviews Materials. Available online: <https://www.nature.com/articles/natrevmats201680> (accessed on 11 September 2023).
53. Huang, Q.; Li, H.; Grätzel, M.; Wang, Q. Reversible Chemical Delithiation/Lithiation of LiFePO₄: Towards a Redox Flow Lithium-Ion Battery. *Phys. Chem. Chem. Phys.* **2013**, *15*, 1793–1797. [[CrossRef](#)] [[PubMed](#)]
54. Pan, F.; Yang, J.; Huang, Q.; Wang, X.; Huang, H.; Wang, Q. Redox Targeting of Anatase TiO₂ for Redox Flow Lithium-Ion Batteries. *Adv. Energy Mater.* **2014**, *4*, 1400567. [[CrossRef](#)]
55. Jia, C.; Pan, F.; Zhu, Y.G.; Huang, Q.; Lu, L.; Wang, Q. High-Energy Density Nonaqueous All Redox Flow Lithium Battery Enabled with a Polymeric Membrane. *Sci. Adv.* **2015**, *1*, e1500886. [[CrossRef](#)] [[PubMed](#)]

56. Fan, F.Y.; Woodford, W.H.; Li, Z.; Baram, N.; Smith, K.C.; Helal, A.; McKinley, G.H.; Carter, W.C.; Chiang, Y.-M. Polysulfide Flow Batteries Enabled by Percolating Nanoscale Conductor Networks. *Nano Lett.* **2014**, *14*, 2210–2218. [[CrossRef](#)]
57. Li, J.; Yang, L.; Yang, S.; Lee, J.Y. The Application of Redox Targeting Principles to the Design of Rechargeable Li–S Flow Batteries. *Adv. Energy Mater.* **2015**, *5*, 1501808. [[CrossRef](#)]
58. Hatakeyama-Sato, K.; Sadakuni, K.; Kitagawa, K.; Oyaizu, K. Thianthrene Polymers as 4 V-Class Organic Mediators for Redox Targeting Reaction with LiMn_2O_4 in Flow Batteries. *Sci. Rep.* **2023**, *13*, 5711. [[CrossRef](#)]
59. Herren, F.; Fischer, P.; Ludi, A.; Haelg, W. Neutron Diffraction Study of Prussian Blue, $\text{Fe}_4[\text{Fe}(\text{CN})_6]_3 \cdot x\text{H}_2\text{O}$. Location of Water Molecules and Long-Range Magnetic Order. *Inorg. Chem.* **1980**, *19*, 956–959. [[CrossRef](#)]
60. Schröter, E.; Stolze, C.; Saal, A.; Schreyer, K.; Hager, M.D.; Schubert, U.S. All-Organic Redox Targeting with a Single Redox Moiety: Combining Organic Radical Batteries and Organic Redox Flow Batteries. *ACS Appl. Mater. Interfaces* **2022**, *14*, 6638–6648. [[CrossRef](#)] [[PubMed](#)]
61. Zhou, M.; Huang, Q.; Pham Truong, T.N.; Ghilane, J.; Zhu, Y.G.; Jia, C.; Yan, R.; Fan, L.; Randriamahazaka, H.; Wang, Q. Nernstian-Potential-Driven Redox-Targeting Reactions of Battery Materials. *Chem* **2017**, *3*, 1036–1049. [[CrossRef](#)]
62. Chen, Y.; Zhou, M.; Xia, Y.; Wang, X.; Liu, Y.; Yao, Y.; Zhang, H.; Li, Y.; Lu, S.; Qin, W.; et al. A Stable and High-Capacity Redox Targeting-Based Electrolyte for Aqueous Flow Batteries. *Joule* **2019**, *3*, 2255–2267. [[CrossRef](#)]
63. Cheng, Y.; Wang, X.; Huang, S.; Samarakoon, W.; Xi, S.; Ji, Y.; Zhang, H.; Zhang, F.; Du, Y.; Feng, Z.; et al. Redox Targeting-Based Vanadium Redox-Flow Battery. *ACS Energy Lett.* **2019**, *12*, 3028–3035. [[CrossRef](#)]
64. Kwabi, D.G.; Ji, Y.; Aziz, M.J. Electrolyte Lifetime in Aqueous Organic Redox Flow Batteries: A Critical Review. *Chem. Rev.* **2020**, *120*, 6467–6489. [[CrossRef](#)]
65. Zhou, M.; Chen, Y.; Salla, M.; Zhang, H.; Wang, X.; Mothe, S.R.; Wang, Q. Single-Molecule Redox-Targeting Reactions for a pH-Neutral Aqueous Organic Redox Flow Battery. *Angew. Chem. Int. Ed.* **2020**, *59*, 14286–14291. [[CrossRef](#)]
66. Huang, S.; Zhang, H.; Salla, M.; Zhuang, J.; Zhi, Y.; Wang, X.; Wang, Q. Molecular Engineering of Dihydroxyanthraquinone-Based Electrolytes for High-Capacity Aqueous Organic Redox Flow Batteries. *Nat. Commun.* **2022**, *13*, 4746. [[CrossRef](#)] [[PubMed](#)]
67. Wong, C.M.; Sevov, C.S. All-Organic Storage Solids and Redox Shuttles for Redox-Targeting Flow Batteries. *ACS Energy Lett.* **2021**, *6*, 1271–1279. [[CrossRef](#)]
68. Yu, J.; Salla, M.; Zhang, H.; Ji, Y.; Zhang, F.; Zhou, M.; Wang, Q. A Robust Anionic Sulfonated Ferrocene Derivative for pH-Neutral Aqueous Flow Battery. *Energy Storage Mater.* **2020**, *29*, 216–222. [[CrossRef](#)]
69. Zhang, J.; Yan, Y.; Wang, X.; Cui, Y.; Zhang, Z.; Wang, S.; Xie, Z.; Yan, P.; Chen, W. Bridging Multiscale Interfaces for Developing Ionically Conductive High-Voltage Iron Sulfate-Containing Sodium-Based Battery Positive Electrodes. *Nat. Commun.* **2023**, *14*, 3701. [[CrossRef](#)]
70. DeBruler, C.; Hu, B.; Moss, J.; Luo, J.; Liu, T.L. A Sulfonate-Functionalized Viologen Enabling Neutral Cation Exchange, Aqueous Organic Redox Flow Batteries toward Renewable Energy Storage. *ACS Energy Lett.* **2018**, *3*, 663–668. [[CrossRef](#)]
71. Hu, B.; Tang, Y.; Luo, J.; Grove, G.; Guo, Y.; Liu, T.L. Improved Radical Stability of Viologen Anolytes in Aqueous Organic Redox Flow Batteries. *Chem. Commun.* **2018**, *54*, 6871–6874. [[CrossRef](#)] [[PubMed](#)]
72. Liu, W.; Liu, Y.; Zhang, H.; Xie, C.; Shi, L.; Zhou, Y.-G.; Li, X. A Highly Stable Neutral Viologen/Bromine Aqueous Flow Battery with High Energy and Power Density. *Chem. Commun.* **2019**, *55*, 4801–4804. [[CrossRef](#)] [[PubMed](#)]
73. Zhou, M.; Chen, Y.; Zhang, Q.; Xi, S.; Yu, J.; Du, Y.; Hu, Y.-S.; Wang, Q. $\text{Na}_3\text{V}_2(\text{PO}_4)_3$ as the Sole Solid Energy Storage Material for Redox Flow Sodium-Ion Battery. *Adv. Energy Mater.* **2019**, *9*, 1901188. [[CrossRef](#)]
74. Meyerson, M.L.; Rosenberg, S.G.; Small, L.J. A Mediated Li–S Flow Battery for Grid-Scale Energy Storage. *ACS Appl. Energy Mater.* **2022**, *5*, 4202–4211. [[CrossRef](#)]

Disclaimer/Publisher’s Note: The statements, opinions and data contained in all publications are solely those of the individual author(s) and contributor(s) and not of MDPI and/or the editor(s). MDPI and/or the editor(s) disclaim responsibility for any injury to people or property resulting from any ideas, methods, instructions or products referred to in the content.